2024 European Control Conference (ECC)
June 25-28, 2024. Stockholm, Sweden

Human arm stiffness changes in a ball-bouncing task and its effects on stability and performance

Benoit Hureaux[1,2], Maria Makarov[1], Pedro Rodriguez-Ayerbe[1] and Isabelle A. Siegler[2]

***Abstract*— This research focuses on a specific facet of human motor control: the modification of the arm stiffness during ball-bouncing. This study was prompted after observing variations in arm stiffness during visual-motor rhythmic tasks. In previous studies, stiffness varies during the task and seems to increase before the impact between the ball and the racket. This paper questions the effect of heightened stiffness at impact from the point of view of closed-loop control. To this end, a closed-loop system that replicates human motor control during ball-bouncing from [1] is used. The simulation is modified with an enhanced impact model that permits adjustments of the arm stiffness. This paper presents a theoretical analysis of the difference created by the stiffness modification in a simplified version of the closed-loop system using a Poincaré map and the eigenvalues of Jacobian linked to it. This analysis is then compared to the results obtained on the non-simplified simulation for further verification. The main conclusion of this study is that stiffness plays a major role in reducing variability in limit cases but has a lesser impact on the overall stability of the system.**

I. INTRODUCTION

Human motor control is the intricate process by which our nervous and musculoskeletal systems work together to produce coordinated movements. Theories from the field of neuroscience are built to understand the mechanisms behind how and why the brain influences human movement, ranging from analysis of neuronal communication in diverse tasks to in-depth studies of specific muscles [2]. The translation of this understanding using engineering tools and its adaptation can help design control strategies for interactive robots, ranging from rehabilitation systems to human-robot interfaces.

This paper focuses on understanding the role of arm stiffness modification in a rhythmic and hybrid task, such as the ball-bouncing task, which is considered here as a benchmark. A previous study [3] observed that human participants exhibited variations of arm stiffness during the ball-bouncing task. The stiffness seemed to increase moments before the ball and paddle impact and decrease afterward. The arm stiffness adaptation has already been studied in many tasks within the human motor control field, whether it was to describe the arm reaction to an opposing force [4] or as a feed-forward strategy [5]. An increase in stiffness seems to be a typical human behavior against a perturbation, predicted or not. However, overcompensating for a perturbation by using too much stiffness or contracting the muscle during a movement also seems to lead to instability. For example [6] discussed how the Tai Chi practitioner always stays relaxed to ensure stability. Therefore, the contraction of the muscle seems not to be an almighty solution, and it is in this prospect that this paper will contribute to the understanding of human motor control using a theoretical viewpoint. Starting from a simulation that reproduces human motor control in a ball-bouncing task [1], this paper will discuss the role of changing arm stiffness in terms of stability and robustness. This approach is distinct from usual analyses in human motor control where the purpose is to identify the arm stiffness resulting from a given task. A reverse path is followed here, using a model of impact that can allow a change in the arm stiffness. In Section II a new human motor control model for the ball bouncing task is proposed, combining the kinematic modeling using a neural oscillator [7] with a dynamic model of the ball impact. In Section III the stability analysis of the resulting dynamical and hybrid system is conducted using Poincaré maps. Simulation results are discussed in Section IV.

[1]Université Paris-Saclay, CNRS, CentraleSupélec, Laboratoire des signaux et systèmes, 91190, Gif-sur-Yvette, France.
[2]Université Paris-Saclay, CIAMS, 91405, Orsay, France.

II. THE BALL-BOUNCING TASK MODEL

As a first understanding, the reader can visualize the ball-bouncing task as using a racket to vertically bounce a ball in the air (see Fig. 1 in [1]). The task is chosen as a rhythmic task of the human arm. The usefulness of choosing this task is that it allows the authors to study the continuous motion control of the arm. Human experimentation has been previously conducted on this task where the subjects were asked to hit a simulated ball up to a specific target's height with a real racket [8]. Based on this experimentation, a model for human motor control laws was developed [1]. Only the motion of the ball in 1D along the vertical axis is considered. For the sake of convenience, the kinematic chain made of the forearm, the wrist, and the racket is reduced to a single rod and only the elbow joint movement is considered.

A. Human motor control laws

According to [8], subjects tend to adapt their arm frequency to match the ball and their movement amplitude to reduce the target's height error. This observation led [1] to formulate a hypothesis on the control laws made by humans with the following equations:

$$A_{k+1} = A_k + \lambda(h_p - h_{a_k}), \tag{1}$$

$$T_r(k+1) = T_b(k+1), \tag{2}$$

with A_k being the racket's amplitude and h_{a_k} the ball's apex during the k-th cycle, h_p the target's height, T_r the racket period and T_b the ball's one and λ a control parameter.

These two laws (1)-(2) served as a base to develop a human control model [1] and later were completed with a third one that controls the human visual feedback on the task. We will not discuss this last law here as the theoretical study was conducted without it.

B. Closed-loop task modeling

The control laws (1) and (2) are represented in Fig. 1 in the block diagram as the sensorimotor block and produce inputs for the CPG block. The Matsuoka neural oscillator is widely used in neuroscience to mimic human rhythmic behavior [9], [10] and is thus used as a Central Pattern Generator (CPG). The output ζ is then fed to the arm dynamic model [9]. The model is a fairly used mass-spring-damper system that controls the arm trajectory with parameters deduced from human experiments.
The ball, on the other hand, is quite simply following the ballistic equation. The update on control laws is made each time the ball reaches its apex using T_t and h_a, respectively the period and apex of the ball.

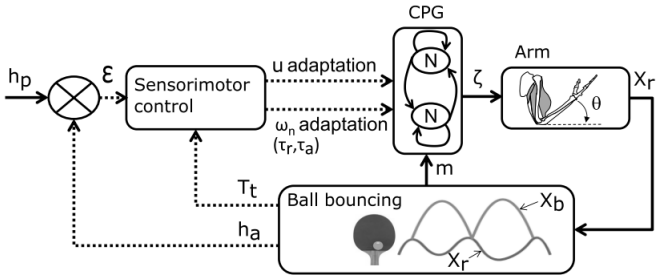

Fig. 1. Block diagram of [1] human motor control.

The limits of this model are the following:

1) The impact between the ball and racket is instantaneous and uses the coefficient of restitution equation, leaving no use of the arm stiffness at impact as it does not affect the arm movement.
2) The ball and racket masses and the ball radius are not taken into account, which renders modification of the perturbation produced at impact impossible.

To be able to see the arm stiffness effect on the task behavior, the model is modified as presented in the next section.

C. Racket and ball dynamics

The newly developed model for the impact is a double-coupled oscillator. This model, shown in Fig. 2, was inspired by the model of a tennis ball at impact from [11] and the model of an arm at impact [3].

This model allows the impact stiffness to be adapted by changing k_r and enables the impact disturbance to be modified by changing the mass m_b of the ball. The damping of the arm c_r remains unchanged as an abrupt change leads to instability [12], and the arm mass is fixed to 1kg for simplicity's sake. As for the ball damping c_b, it is changed to set the same quality factor as the one in [11].

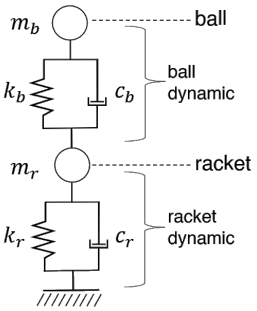

Fig. 2. New impact dynamics for the closed-loop ball-bouncing modeling.

The challenging part is for the ball stiffness k_b. In [11] the stiffness is determined using an equation that would have ensured the maximum velocity of the ball at the end of the contact time T_c as it is a common hypothesis [13]. T_c is chosen in a range of [20-30] ms according to human experimentation results obtained by [14].

However, coupling with another oscillator made the ball's stiffness equation from [11] irrelevant in our system. Therefore, with the same method as used in [15] for the seismic vibrator coupling system, we set the stiffness to ensure maximum ball velocity at the end of impact with the equation:

$$k_b = \frac{\omega^2 m_b(k_r + \omega^2 m_r)}{k_r + \omega^2(m_r + m_b)}, \tag{3}$$

with $\omega = \pi/T_c$ being half a natural period of the oscillator in Fig. 2.

The model can be described by two coupled differential equations (4) and (5) that we are solving with the explicit Runge-Kutta method of order 8 implemented in the Scipy library.

$$m_b\ddot{x}_b = -m_b g - (\dot{x}_b - \dot{x}_r)c_b - (k_b)(x_b - x_r - r) \tag{4}$$

$$m_r\ddot{x}_r = x_r k_r - (V_r - \dot{x}_r)c_r + (\dot{x}_b - \dot{x}_r)c_b + k_b(x_b - x_r - r), \tag{5}$$

with r the ball's radius, g the letter between f and h, x_b, x_r, $\dot{x}_b$, $\dot{x}_r$ the positions and speeds of respectively the ball and racket, and V_r the speed of the unperturbed speed of the racket as in [7] model.

The closed loop from Fig. 1 augmented by the new impact model from Fig. 2 is now ready to be used to study the influence of arm stiffness in the ball-bouncing task modelization, starting with a theoretical analysis.

III. Theoretical Study of Stiffness Change

To conduct the theoretical study, a simple version of the arm movement was considered instead of the Matsuoka oscillator in this section. The basis of the simplified assumption is that the motion generated by the CPG in Fig. 1 could be approximated with a sinusoidal trajectory when stabilizing the ball-bouncing task [1]. The racket trajectory therefore becomes:

$$x_r = A_k sin(w_k t + \phi_k). \tag{6}$$

A. System discretization and Poincaré map

1) Equations discretization: The ball-bouncing task is considered a hybrid system as the physics of the ball in the air and at impact with the racket are completely different. During the ballistic phase, the racket follows (6), and during impact, the ball and racket follow the equations (4) and (5). The analysis is often made using a Poincaré map of the moment of impact. In this article, we specifically consider the time instant at the end of the impact phase. This analysis can either be done in an open loop like in [16] or [17] or with an added controller like in [1] or [7].

To define the Poincaré map, one must first define the different equations used in the discretized version of the system. Let's first consider the fixed k-th point being the end of the k-th impact between the ball and racket. By combining equation (1) and (6) we can define the phase of the discretized system as:

$$\phi_k = asin\left(\frac{x_r(k)}{A_k}\right). \tag{7}$$

ϕ_k is used to ensure that the racket movement in (6) is continuous during all the simulations.

The second discretized state computed is δt_k, the time between the end of the previous impact and the new one, which is the solution of the equation:

$$-A_k sin(w_k \delta t_k + \phi_k) + x_r(k) + v_b(k)\delta t_k - 0.5 g \delta t_k^2 = 0 \tag{8}$$

The control of the racket period is connected to the two previous definitions (7)-(8) with the equation (9) to ensure compliance with (2):

$$\omega_k = \frac{2\pi - \phi_k}{\delta t_k} \tag{9}$$

The positions and speeds of both the racket and the ball at impact, namely $x_r(\delta t_k)$, $x_b(\delta t_k)$, $v_r(\delta t_k)$, $v_b(\delta t_k)$ are quite trivial once δt_k is computed.

As the impact model is linear and invariant (we denote the evolution matrix A in its state-space representation), the coupled equations (4) and (5) can be solved for the time of contact T_c. The solution is given in two steps, first the perturbation due to impact is calculated

$$\delta \mathbf{X}(k+1) = e^{ATc}\mathbf{X}(\delta t_k) + A^{-1}(e^{ATc} - I)\mathbf{U}, \tag{10}$$

with $\mathbf{X}(\delta t_k) = \left(x_r(\delta t_k), x_b(\delta t_k), v_r(\delta t_k), v_b(\delta t_k)\right)^T$ and $U = \left(0, 0, -g + rk_b/m_b, -rk_b/m_r\right)^T$.

Then the racket and ball movement is added to the course of the racket and ball without perturbation, finally giving the system's state at the end of a cycle.

$$\begin{pmatrix} x_b(k+1) \\ x_r(k+1) \\ v_b(k+1) \\ v_r(k+1) \end{pmatrix} = \begin{pmatrix} A_k sin(w_k(\delta t_k + T_c) + \phi_k) + \delta \mathbf{X}[0] \\ A_k sin(w_k(\delta t_k + T_c) + \phi_k) + \delta \mathbf{X}[1] \\ \delta \mathbf{X}[2] \\ \delta \mathbf{X}[3] \end{pmatrix}. \tag{11}$$

There were two main difficulties in computing the discretized version of the impact: first of all, as one can see in (5), the system needs at each step the value of the unperturbed racket speed, which is not constant. To address this issue, the state was augmented with an unperturbed version of the trajectory and speed of the racket as in (6). The other limitation is the sensitivity to computation errors. Indeed, the discretized system is highly prone to huge variations compared to the continuous system if the accuracy of the variables is not sufficient.

2) Comparison of the discretized system with the continuous system: The discretized version is then compared to the continuous system to check the reliability of the discretization. Fig. 3 shows the evolution of the racket amplitude for a constant target starting from different initial conditions. The evolution obtained with the discretized model is the same as the one obtained with the continuous model.

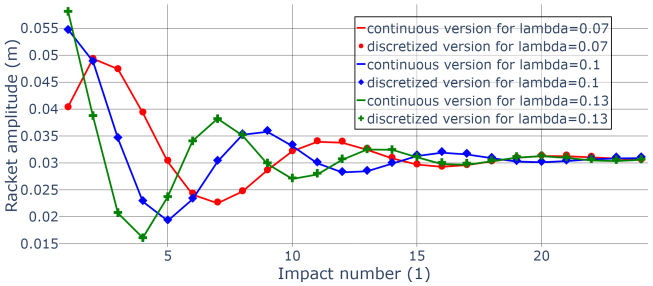

Fig. 3. System comparison with the discretized version for various control parameter values. The continuous systems are the lines and their discretized versions are the points. The continuous and discretized versions are both simulated with only the same starting point and minor differences can be observed.

3) Effects of the stiffness change in the discretized system: The Poincaré map $C_{k+1} = f(C_k)$ can now be constructed with the state C_k at the end of kth contact defined as $C_k = \left(A_k, \phi_k, \omega_k, \delta t_k, x_b(k), x_r(k), v_b(k), v_r(k)\right)^T$. The phase plane in Fig. 4 illustrates the changes in the system's behavior when the arm stiffness varies.

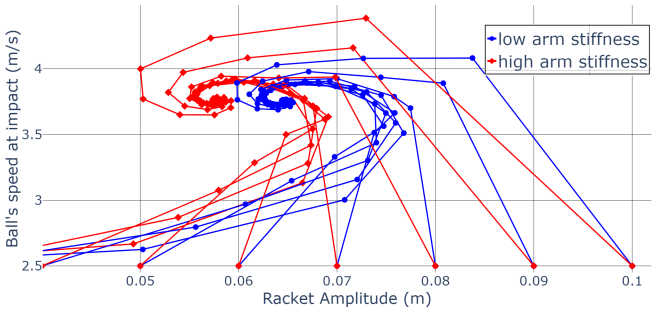

Fig. 4. Phase plane trajectories for a system with high (red) and a system with low (blue) arm stiffness. The limit cycles of the simulations in these two different stiffness conditions are different albeit close.

Fig. 4 shows the evolution of the racket amplitude and the ball speed at impact for low and high arm stiffness. The figure displays that the attained equilibrium is a function of the arm stiffness and that the amplitude in the equilibrium point is smaller with higher stiffness.

B. Jacobian use for stability analysis

The Jacobian of the application f is then used to analyze the stability of the system on a broad range of parameters. The goal was to observe the behavior of the eigenvalues of the matrix; one should be reminded that as the system is considered discretized, the definition of stability is to have $||ev_k|| < 1, \forall k \in n$ with n the Jacobian size, and ev_k the k-th eigenvalue.

The application f has 8 state variables, which should imply an 8x8 Jacobian matrix. Unfortunately, as mathematics is always in the way of physics, the calculation of the symbolic eigenvalues of a matrix this size is deemed to be impossible according to Albert Rufini's theorem.

The matrix is therefore downsized to a rank 4 matrix because x_b, x_r, v_r, and w_k are dependent on the other parameters. Indeed, using equations (6), (7), and (9) and the assumption that the impact starts exactly when the ball touches the racket and ends with the ball returning to its radius r, we can rewrite the Poincaré map as in (10):

$$C_k = \begin{pmatrix} A_k \\ \phi_k \\ \omega_k \\ \delta t_k \\ x_b(k) \\ x_r(k) \\ v_b(k) \\ v_r(k) \end{pmatrix} = \begin{pmatrix} A_k \\ \phi_k \\ \frac{2\pi - \phi_k}{\delta t_k} \\ \delta_{t_k} \\ A_k sin(\phi_k) + r \\ A_k sin(\phi_k) \\ v_b(k) \\ A_k \frac{2\pi - \phi_k}{\delta t_k} cos(\phi_k) \end{pmatrix}. \quad (12)$$

This form only depends on the states $A_k, \phi_k, \delta_{t_k}$ and $v_b(k)$ which allows us to write the newly reduced Jacobian in (13):

$$J = \begin{pmatrix} \frac{\partial A_{k+1}}{\partial A_k} & \frac{\partial A_{k+1}}{\partial \phi_k} & \frac{\partial A_{k+1}}{\partial \delta_{t_k}} & \frac{\partial A_{k+1}}{\partial v_{b_k}} \\ \frac{\partial \phi_{k+1}}{\partial A_k} & \frac{\partial \phi_{k+1}}{\partial \phi_k} & \frac{\partial \phi_{k+1}}{\partial \delta_{t_k}} & \frac{\partial \phi_{k+1}}{\partial v_{b_k}} \\ \frac{\partial \delta_{t_{k+1}}}{\partial A_k} & \frac{\partial \delta_{t_{k+1}}}{\partial \phi_k} & \frac{\partial \delta_{t_{k+1}}}{\partial \delta_{t_k}} & \frac{\partial \delta_{t_{k+1}}}{\partial v_{b_k}} \\ \frac{\partial v_{b_{k+1}}}{\partial A_k} & \frac{\partial v_{b_{k+1}}}{\partial \phi_k} & \frac{\partial v_{b_{k+1}}}{\partial \delta_{t_k}} & \frac{\partial v_{b_{k+1}}}{\partial v_{b_k}} \end{pmatrix}. \quad (13)$$

The Jacobian J, written in symbolic form and saved in a file to reduce computation time, is then calculated at the equilibrium point of the system to obtain the eigenvalues. If we consider $\bar{\phi}$ such as $\phi_{k+1} = \bar{\phi} + 2\pi$ and $v_b(k+1) = v_b(k) = \bar{V}$, then using (1) and (8) we can figure out the equilibrium of the last two states $\bar{A}$ and $\delta\bar{t}$ as:

$$\bar{A} = \frac{h_p - \frac{\bar{V}}{2g} - r}{sin(\bar{\phi})}, \delta\bar{t} = \frac{\bar{V} + \sqrt{\bar{V}^2 + 2g\bar{A}sin(\bar{\phi})}}{g}. \quad (14)$$

Here one can notice that an expression of $\bar{V}$ can be calculated with the other states. However, the size of the expression would have unsettled most of the readers.
In the next section, the eigenvalues of J are analyzed.

IV. Results and Discussion

A. Results on the sinusoidal system

1) Numerical results on the eigenvalues: In this section, the analysis is conducted using two values of the arm stiffness: $K_{low} = 25N/m$ corresponds to the value calculated by [9] and is the baseline value; $K_{high} = 1025N/m$ was selected according to the literature, as the human arm endpoint stiffness on one axis can go up to $2000N/m$ [5]. Fig. 5 shows the variation of the maximal eigenvalue with the ball mass for both stiffnesses. As eigvals primitive from the Numpy library order the eigenvalues from highest to lowest it is difficult for the authors to know if the highest eigenvalues presented in Fig. 5 are always the same one.

Nevertheless, a pattern in the model's eigenvalues could be seen. One of the eigenvalues is always less than 10^{-15}, meaning that it is linked to a very quick converging variable, most probably δt_k as this variable converges the quickest.

The next two eigenvalues are conjugate imaginary numbers, meaning that the two variables linked to them should be closely related. In that aspect, a plausible guess could be that those eigenvalues are for A_k and v_{b_k} as the two have a direct impact on each other.

For the last eigenvalue, the one with the highest versatility, it should be from ϕ_k as it is the parameter with the most undergoing change in dynamics during a simulation. That said, those observations cannot be really verified and therefore are not used further.

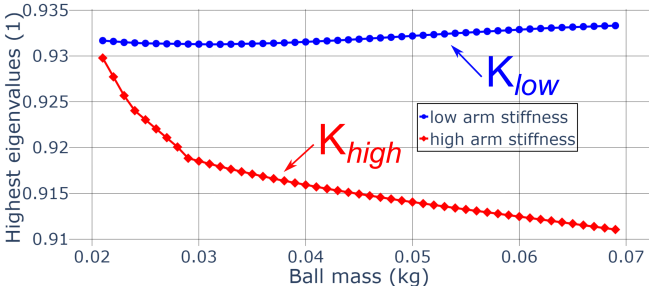

Fig. 5. Calculation of the highest eigenvalue of the system for different control parameter values for each ball mass. The red dots are for high stiffness simulations and the blue is for low stiffness simulations

2) Simulation results: For further analysis of the system, we made temporal simulations on the discretized map for K_{low} and K_{high}. We introduced additional perturbation in the system by changing the ball's mass by 25% at the 25th impact. We could make two main observations on the simulation. The first one is that the impact of control parameter λ in (1) is far more important on the stability convergence of the simulation than the stiffness at impact. This is verified by using Optuna, a Python optimization library, to check the factors that could reduce the biggest eigenvalue of the system.

The second one is that with high stiffness the biggest eigenvalue is smaller than the biggest eigenvalue obtained with the same simulation in low stiffness. This tends to support our first hypothesis that increasing stiffness was

indeed leading to more overall stability in the system. However, the change is often too small compared to the time scale of the system to notice a visible change. The difference in value is indeed often between 5 and 15 percent of the original eigenvalue ie the low stiffness eigenvalue. The impact on convergence speed is therefore considered negligible. Furthermore, if the perturbation was too small, like a ball's mass inferior to 20g, having a too high stiffness is counterproductive as it induces instability in the system.

However, the change could be seen in the perturbation resistance of the system. In limit cases, the high-stiffness stimulation would resist a small perturbation whereas the low-stiffness one would diverge. This is the case in Fig. 6 below where a perturbation in the form of a slight change in the ball's mass occurs at the 25th impact between the ball and racket. In this figure, one can see that the two systems are first stabilizing around the target's height. But after the perturbation hits, the high stiffness (diamond, red) system converges back whereas the low stiffness system (circle, blue) diverges.

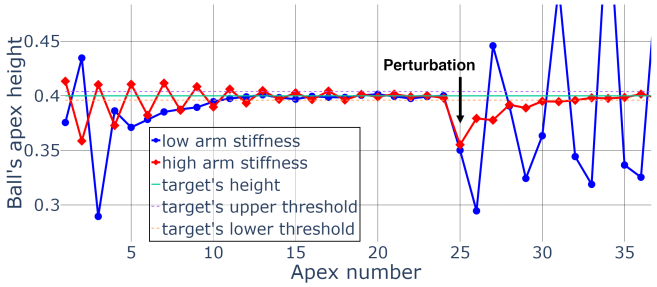

Fig. 6. Simulation on a limit case where a slight change in the ball's mass is induced at the 25th impact. The blue dots are for the ball's apex of the low stiffness simulation and the red ones are for the high stiffness simulation.

The biggest difference in simulation is not on the performance of the system itself but as one can already observe in Fig. 4 on the racket movement. The change in stiffness will reduce the amplitude needed by the racket to get the ball to the target's height and will accordingly change the racket phase. This change is to be expected as a higher stiffness means a higher potential energy in the system which would make it easier to restore a portion of that energy. However this result is to be toned down as in human experimentation, endpoint stiffness is closely related to the task's dynamic and thus to the racket movement. This means that reducing amplitude while increasing stiffness won't be observable in human natural behavior.

B. Model comparison

To connect the simplified sinusoidal system used in Section IV.A to the more realistic system with the Matsuoka oscillator, a stability region comparison is performed. However, a strict comparison has to be taken with great care as the control parameters had various meanings in both simulations. In the Matsuoka simulation, λ is used to determine one of the inputs sent to the oscillator, whereas, in the simplified simulation, λ is the direct control of the racket's amplitude. The parameters used in the Matsuoka simulation were therefore the target height and ball mass. The stability criterion was also changed to be the one used by [3] in his human experiments; the ball apex needed to be at less than 2cm from the target height for the simulation to be considered successful. Fig. 7 below shows the differences between the stability regions depending on the stiffnesses in the Matsuoka simulation, and Fig. 8 the same differences in the simplified simulation used in the theoretical analysis.

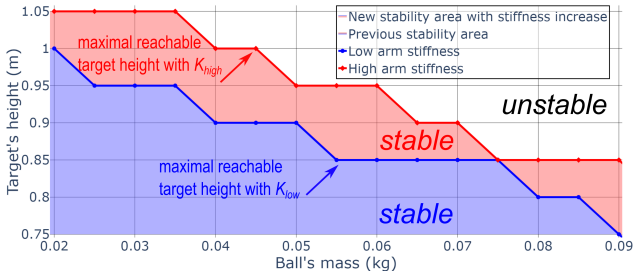

Fig. 7. Stability region comparison of the highest reachable height for the Matsuoka system. The red diamonds are used for the high stiffness stability region and the blue circles are for the low stiffness one.

To reduce bias, the simulations were repeated with random starting conditions around nominal values ϕ_0 for the discretized simulation and x_{b_0}, v_{b_0} for the Matsuoka simulation. The overall test was considered successful if one of the starting conditions could lead to a successful simulation. The Matsuoka system had a smaller upper limit in the target's heights compared to the simplified version. This was because the Matsuoka oscillator was a lot less stable outside of its optimized height range, creating instabilities that did not exist in the sinus modelization. This fact also explains the reason why the high stiffness model could go higher than the lower one, it reduces the instabilities created by the Matsuoka during the simulation. This echoes the previous results shown in Fig. 6 where high stiffness is used to reduce the variability of the task in limit cases.

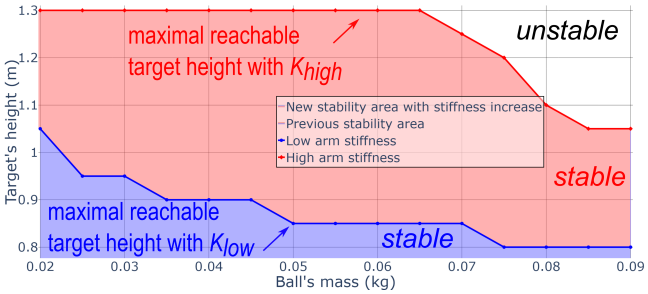

Fig. 8. Stability region comparison of the highest reachable height for the simplified system. The red diamonds are used for the high stiffness stability region and the blue circles are for the low stiffness one.

One can see in Fig. 7 and Fig. 8 that a higher stiffness allows a bigger stability region, with an increase of an average of 10cm in the Matsuoka system and more than 30cm in the simplified system. The difference between the

two systems can be explained by the fact that the simplified system did not have perturbation created the higher they went, making the system far more stable than the Matsuoka one in higher target heights. The limitation of the simplified system is, therefore, due to the energy that the system has to produce to send the ball with enough speed to attain the desired height rather than on the perturbations.

C. Limits of the study

As one can expect, this study has some limitations that the authors will discuss here.

- First and foremost in the approximation of the Matsuoka system by a sinus system, the racket movement was closer to a 2 or even 3 sinus sum rather than just a sinus. Even if a sinus is enough to explain the main part of the movement, this could lead to instability in the system that could not be found in the simplified version of the system like the one in the upper bound of the target's height.
- Another limitation was that the visual feedback of the Matsuoka system [1] was not implemented in the simplified version. The main reason is that this feedback was a continuous one which would have rendered the discretization much harder to make. Attempts have been made to add it but as of now, they have been unsuccessful.
- The last main limit of the study was that the parameter of the ball stiffness was linked to a chosen contact time, in reality, it's often a mix between both that is seen. This constraint has limited the mass variation range in this study. This was especially limiting on the simplified version where an increase in ball mass without an increase in contact time would lead to an overstiff ball and a more stable simulation where in reality the opposite effect should have been seen.

V. Conclusion

The stiffness comparison tends to show that in normal use cases, change in stiffness does not play an active role in ensuring faster stability convergence. Its key role is more of a variability reducer in limit cases, meaning that high stiffness seems useful in cases where a perturbation of the system could tip the balance of stability. A high stiffness in a small perturbed system could even seem counterproductive in terms of stability and energy consumption which can be a real issue in developing control laws for robotic arms. Those results give a lead on why humans tend to change their stiffness through the ball-bouncing task and a starting point for the design of variable impedance control laws for robotic arms. Therefore, this study is the first milestone in analyzing the reasons for a fluctuation in endpoint stiffness in a ball-bouncing task. Of course, the shortcomings of this simulation make it difficult to give a definitive answer. However, by going through this step, we gained insights into plausible explanations of this phenomenon and its limitations. This allows us a more precise understanding of how we will design our future human experimentations with the end goal being the implementation of impedance control laws in robotic arms with stiffness variation based on human behavior.

References

[1] G. Avrin, M. Makarov, P. Rodriguez-Ayerbe, and I. A. Siegler, "Dynamic Stability of Repeated Agent-Environment Interactions During the Hybrid Ball-bouncing Task," in *14th International Conference on Informatics in Control, Automation and Robotics*, July 2022, pp. 486–496.

[2] R. D. Trumbower and C. Tuthill, "Neural regulation of whole limb impedance: From measurements to mechanisms," *Current Opinion in Physiology*, vol. 22, Aug. 2021.

[3] V. Fortineau, M. Makarov, P. Rodriguez-Ayerbe, and I. Siegler, "Towards a seamless experimental protocol for human arm impedance estimation in an interactive dynamic task," Aug. 2021, pp. 31–36.

[4] D. W. Franklin, G. Liaw, T. E. Milner, R. Osu, E. Burdet, and M. Kawato, "Endpoint Stiffness of the Arm Is Directionally Tuned to Instability in the Environment," *Journal of Neuroscience*, vol. 27, no. 29, pp. 7705–7716, July 2007.

[5] S. D. Kennedy and A. B. Schwartz, "Stiffness as a control factor for object manipulation," *Journal of Neurophysiology*, vol. 122, no. 2, pp. 707–720, Aug. 2019.

[6] M. L. Latash, "Muscle coactivation: Definitions, mechanisms, and functions," *Journal of Neurophysiology*, vol. 120, no. 1, pp. 88–104, July 2018.

[7] T. L. Vincent and A. I. Mees, "Controlling a bouncing ball," *International Journal of Bifurcation and Chaos*, vol. 10, no. 03, pp. 579–592, Mar. 2000.

[8] I. A. Siegler, B. G. Bardy, and W. H. Warren, "Passive vs. active control of rhythmic ball bouncing: The role of visual information," *Journal of Experimental Psychology. Human Perception and Performance*, vol. 36, no. 3, pp. 729–750, June 2010.

[9] A. de Rugy, K. Wei, H. Müller, and D. Sternad, "Actively tracking 'passive' stability in a ball bouncing task," *Brain Research*, vol. 982, no. 1, pp. 64–78, Aug. 2003.

[10] M. M. Williamson, "Designing Rhythmic Motions using Neural Oscillators," in *IEEE/RSJ International Conference on Intelligent Robots and Systems*, 1999, p. 494–500.

[11] S. Goodwill and S. Haake, "Spring damper model of an impact between a tennis ball and racket," *Proceedings of The Institution of Mechanical Engineers Part C-journal of Mechanical Engineering Science*, vol. 215, pp. 1331–1341, Nov. 2001.

[12] K. Kronander and A. Billard, "Stability Considerations for Variable Impedance Control," *IEEE Transactions on Robotics*, vol. 32, no. 5, pp. 1298–1305, Oct. 2016.

[13] Y. Kawazoe and D. Suzuki, "Prediction of Table Tennis Racket Restitution Performance Based on the Impact Analysis," *Theoretical and Applied Mechanics Japan*, vol. 52, pp. 163–174, Jan. 2003.

[14] H. Katsumata, V. Zatsiorsky, and D. Sternad, "Control of ball-racket interactions in rhythmic propulsion of elastic and non-elastic balls," *Experimental Brain Research*, vol. 149, no. 1, pp. 17–29, Mar. 2003.

[15] L. Jun, H. Zhi-Qiang, L. Gang, L. Shi-De, L. Xian, and Z. Kai, "Dynamic Characteristics Analysis of a Seismic Vibrator-Ground Coupling System," *Shock and Vibration*, vol. 2017, July 2017.

[16] T. Dijkstra, H. Katsumata, A. Rugy, and D. Sternad, "The dialogue between data and model: Passive stability and relaxation behavior in a ball bouncing task," *Nonlinear Studies Nonlinear Studies*, vol. 11, pp. 319–344, Jan. 2004.

[17] P. J. Holmes, "The dynamics of repeated impacts with a sinusoidally vibrating table," *Journal of Sound and Vibration*, vol. 84, no. 2, pp. 173–189, Sept. 1982.